NASA TECHNICAL MEMORANDUM

NASA TM X-71897

NASA TM X-71897

(NASA-TM-X-71897) MAGNETIZATION AND MAGNETIC SUSCEPTIBILITIES OF GdH3, HoH3, ErH3 AND YbH3 (NASA) 14 p HC $3.50 CSCL 20L

N76-22078

Unclas
G3/76 25218

MAGNETIZATION AND MAGNETIC SUSCEPTIBILITIES OF GdH_3, HoH_3, ErH_3 AND YbH_3

by D. J. Flood
Lewis Research Center
Cleveland, Ohio 44135

TECHNICAL PAPER presented at
American Physical Society Meeting
Atlanta, Georgia, March 29-April 2, 1976

MAGNETIZATION AND MAGNETIC SUSCEPTIBILITIES OF GdH_3, HoH_3, ErH_3 AND YbH_3

by D. J. Flood

Lewis Research Center

E-8683

ABSTRACT

The magnetic susceptibility of powdered samples of HoH_3, ErH_3, GdH_3 and YbH_3 have been measured in the temperature range from 4.2 to 1.2 K. Two broad, local maxima are observed in the variation of χ versus T for GdH_3, with maxima in $(\Delta\chi/\Delta T)$ versus T at 1.8 K and 3.3 K. The inverse susceptibilities for HoH_3 and ErH_3 both obey a Curies-Weiss law over a limited range (4.2 to 2.6 K and 4.2 to 2 K respectively) with values for the Weiss constant of -4.25 K and -1.11 K, and effective moments of 8.6 and 7.7 Bohr magnetons respectively. The susceptibility of YbH_3 is independent of temperature over the range investigated. High-field magnetization measurements yield extrapolated saturation moments of $(7.0\pm0.25)\mu_B$ for GdH_3, $(6.1\pm0.2)M_B$ for HoH_3 and $(3.74\pm0.11)\mu_B$ for ErH_3. In addition, ErH_3 exhibits a van Vleck paramagnetism in the high field region.

INTRODUCTION

Wallace and co-workers have shown (1, 2) that the heavy rare-earth trihydrides crystallize in hexagonal close-packed arrangement, as illustrated in figure 1. The addition of hydrogen distorts the lattice in the trihydride phase, resulting in c/a ratios around 1.8, compared with c/a ratios in the pure metals ranging from 1.57 to 1.59. The hydrogen anions reside in the lattice at the tetrahedral and octrahedral sites. Each rare-earth ion has nine nearest-neighbor hydrogen anions, and these in turn form an almost close-packed arrangement in their coordination to one another.

The presence of the hydrogen anions affects the magnetic properties of the rare-earth host in two ways. Since the interactions which produce ferro- and antiferromagnetism in the lanthanides result from indirect exchange, i.e., exchange via the conduction band electrons, the addition of anything which depletes the conduction band should weaken the interaction and thereby lower the magnetic ordering temperature. That such is the case for hydrogen has been reported by Wallace, Kubota and Zanowick (3) and Kubota and Wallace (4). The hydrogen anions also affect the magnetic properties of the host lattice by virtue of the crystalline electric fields they produce at the rare-earth sites. (Crystal field effects in rare earth metals, alloys and compounds are well-known and have been extensively studied. See Refs. 5 and 6 for excellent reviews of some of the fundamental aspects of rare earth magnetism.) Basically, the crystal field removes part of the (2J + 1)-fold degeneracy of the magnetic ground state of the rare earth 4f electrons, separating the previously degenerate levels by energies ranging from the equivalent of a few degrees Kelvin to at most a few hundred degrees Kelvin. The effects of the crystal field should show up in susceptibility and magnetization measurements at low temperatures.

EXPERIMENTAL TECHNIQUES

Magnetic susceptibility measurements have been made as a function of temperature in zero applied field, and in some cases, as a function of applied field at fixed temperature. Standard field-modulation techniques were employed using a 23 hertz modulating field and a phase-sensitive detector. The amplitude of the modulating field was less than 0.5×10^{-4} Tesla (0.5 gauss). The magnetization measurements were made by integrating the output of two search coils which were connected in series-opposition to one another. One of the coils contained the sample while the other was empty. Magnetization studies were made as a function of field at fixed temperatures. All temperatures were in the range 1.2 to 4.2 K, and applied fields ranged to 7 Tesla. All samples were commercially prepared and in powder form. Because they react readily in air

to form oxides, the materials were stored in helium gas. Samples were compacted with the aid of a test tube vibrator into 4 millimeter inside diameter glass tubes which were sealed with a stopper. All samples were approximately 10 centimeters long and the average density of each was determined with a ±4 percent uncertainty. The uncertainty in the density was the largest source of experimental error. The uncertainties in the measurements of χ were typically less than 0.5 percent, and in M typically less than 2 percent.

RESULTS AND DISCUSSION

A. GdH_3

The magnetic susceptibility as a function of temperature is shown in figure 2. The maximum in χ is indicative of antiferromagnetic ordering. The shape of the curve on the low temperature side of the maximum is surprising. The Neel Temperature T_N, is the point where $d\chi/dT$ is a maximum. In figure 3 a plot of $\Delta\chi/\Delta T$ reveals two maxima, one at 3.32 K and the other at 1.8 K. The $\Delta\chi$ were obtained from the data in figure 2 for $\Delta T \simeq 0.1$ K, and the ratio $\Delta\chi/\Delta T$ was plotted at the mid-point of each ΔT. Similar results for χ and $\Delta\chi/\Delta T$ were obtained on two different samples from two different suppliers.

The peak at 3.32 K is probably the result of antiferromagnetic ordering, and the peak at the lower temperature may be ascribable to a structural transformation of some kind. Detailed studies of the specific heat in zero and applied magnetic fields should provide some information on the nature of any phase changes which may be occurring. The limited data in the paramagnetic region preclude an accurate estimate of the effective moment and Weiss constant, except to say that the latter is negative and greater than -8 K. The magnetization as a function of B/T is shown in figure 4, along with a plot of the Brillouin function using the free-ion values $J = 7/2$ and $g_L = 2$. The effects of antiferromagnetic ordering are clearly present. Figure 5 is a plot of M versus B^*/T, where B^* is the internal field given by the Weiss molecular field theory

$B^* = B - \lambda M$. λ is the Weiss molecular field constant. The high-field data lie within experimental error of the Brillouin function. This implies that the saturation moment is $7\,\mu_B$, as would be expected for this compound where crystal field affects are small. λ was computed by determining the value of $(\lambda M/T)$ needed to bring the experimental points in figure 4 into coincidence with the Brillouin function. The value of λ obtained was 62.5 ± 2.5.

B. HoH_3

Figure 6 is a plot of $1/\chi$ versus T. The data indicate the probable presence of an antiferromagnetic transition below 1.2 K. The Curie constant C, computed from the slope of the linear region, yields an effective moment, $P_{eff} = (8.6 \pm 0.3)\mu_B$ per Ho+++ ion, and $\theta = -4.1 \pm 0.4$. (The free-ion value of P_{eff} is $10.6\mu_B$). Magnetization data are shown in figure 7. The high field region for T = 3 K has been fit to within 2 percent by the first rational Padé approximant (7)

$$M = \frac{7.65 \times 10^{-6}(B/T)}{1 + 1.44(B/T)}$$

for $(B/T) \geq 0.75$. The limit of this expression as $B/T \to \infty$ provides an estimate of the saturation moment Jg from $M_s = NgJ\mu_B$ and yields $(6.1 \pm 0.24)\mu_B$ per Ho+++ ion. Calculations by Segal and Wallace (8) indicate that the high field moment for a $J = \pm 5$ ground state is approximately $6.2\,\mu_B$ per ion. (The free ion saturation moment is $10\,\mu_B$). The difference between the low field effective moment and the saturation moment indicates that the zero field ground state is probably not a simple $J = \pm 5$ doublet, however.

C. ErH_3

A plot of $1/\chi$ versus T is shown in figure 8. The susceptibilities were obtained in this case from initial slopes of M versus B. The effective moment is $(7.7 \pm 0.3)\mu_B$ per ion. The intercept, θ, is -1.1 K.

Assuming that the perpendicular component of χ is zero (i.e., $g_\perp = 0$), the powder susceptibility is given by $\chi_p = (1/3)\chi_\parallel$. (Perpendicular and parallel orientations are relative to the applied field direction.) If the ground state is an effective spin one-half doublet, then

$$P_{eff}^2 = \frac{1}{3}\mu_\parallel^2 = \frac{1}{3}\left(g_\parallel^2 \cdot \frac{3}{4}\right)$$

so that $g_\parallel = 15.4$. $\mu_\parallel$ is the component of the ionic magnetic moment parallel to the applied field, and $g_\parallel$ is simply $2g_L\langle J_z\rangle = 2.4\langle J_z\rangle$. g_L is the Lande g- factor. From the above value of $g_\parallel = 15.4$, it is seen that $\langle J_z\rangle \simeq 6.4\pm0.2$. The result strongly suggests a $J_z = \pm 13/2$ doublet ground state. The magnetization is shown in figure 9. The high field region has a temperature-independent slope indicative of van Vleck paramagnetism. Extrapolation from the high field region to $B/T = 0$ yields a saturation moment of $3.74\ \mu_B$. Again, under the assumption that $g_\perp \simeq 0$, the saturation moment per ion is $\mu_p = 1/2\ g_\parallel J'$ where μ_p is the measured saturation moment per ion for a powder, and $J' = 1/2$ is the effective spin. Hence, $g_\parallel = 4\ \mu_p = 14.96$, and $\langle J_z\rangle = 6.2\pm0.2$. This result is in good agreement with the low field result and also implies a $J_z = \pm 13/2$ ground state. Figure 10 is a plot of $M - \alpha B$ versus B/T with $\alpha = (1.6\pm0.2)\times10^{-3}$. The solid line is a plot of the Brillouin function for a doublet level with $g_\parallel = 14.96$. The agreement is excellent.

D. YbH_3

YbH_3 exhibited a small, positive, but temperature independent susceptibility $\chi = 1.2\times10^{-3}$ over the range 4.2 to 1.2 K. The magnetization was also small and independent of temperature. The moment per ion at B = 7 Tesla is $(0.025\pm0.01)\mu_B$. The results indicate the probable existence of a singlet ground state for this compound.

CONCLUSION

Magnetization and magnetic susceptibility measurements on HoH_3, ErH_3, and YbH_3 reveal several of the complex effects of crystalline

electric fields found in many rare earth alloys and compounds. The measurements of GdH_3 on the other hand, indicate, as expected for a magnetic ion with a half-filled electronic shell, that even at 4.2 K crystal field effects are small compared to magnetic interactions between the gadolinium ions. Except for GdH_3, the high field magnetic moment per ion is not in agreement with free ion values for each of the compounds. The table below summarizes these results.

Saturation Moment (Bohr magnetons/ion)

	Observed	Theory
GdH_3	7±0.3	7
HoH_3	6.1±0.24	10
ErH_3	3.74±0.15	9
YbH_3	[a]0.025±0.01	4

[a]Saturation not clearly reached

The data for GdH_3 can be used to estimate the Weiss molecular field constant to be $\lambda = 62.5 \pm 2.5$ for that material. The high field magnetic moment for HoH_3 is consistent with a $J = \pm 5$ ground state, while ErH_3 appears to have a $J = \pm 13/2$ ground state.

REFERENCES

1. M. Mansmann and W. E. Wallace, J. Physique 25, 454 (1964).
2. A. Pebler and W. E. Wallace, J. Phys. Chem. 66, 148 (1962).
3. W. E. Wallace, Y. Kubota, and R. L. Zanowick, in Adv. in Chem. 39, 122, Am. Chem. Soc. (1963).
4. Kubota and W. E. Wallace, J. Chem. Phys. 39, 1285 (1963).
5. T. R. McGuire, IEEE Trans. Magnetics, MAG-8, 105 (1972).
6. B. R. Cooper, Rev Solid State Sci., 3, 83 (1972)
7. A. Baker, Jr., Adv. Theoretical Phys. 1, 1, (1965).
8. E. Segal and W. E. Wallace, J. Solid State Chem. 6, 99 (1973).

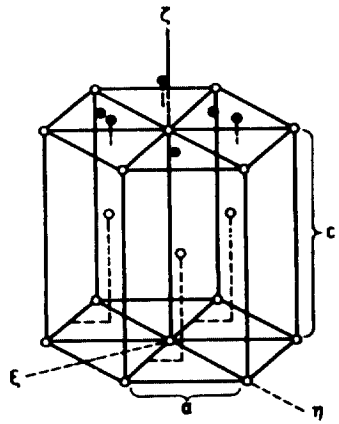

Figure 1. - Hexagonal-close-packed (hcp) structure pertinent to heavy rare earth trihydrides. The ● represent hydrogen anions. Six anions lie at mirror images above and below the basal plane, and three lie almost in, but slightly above it.

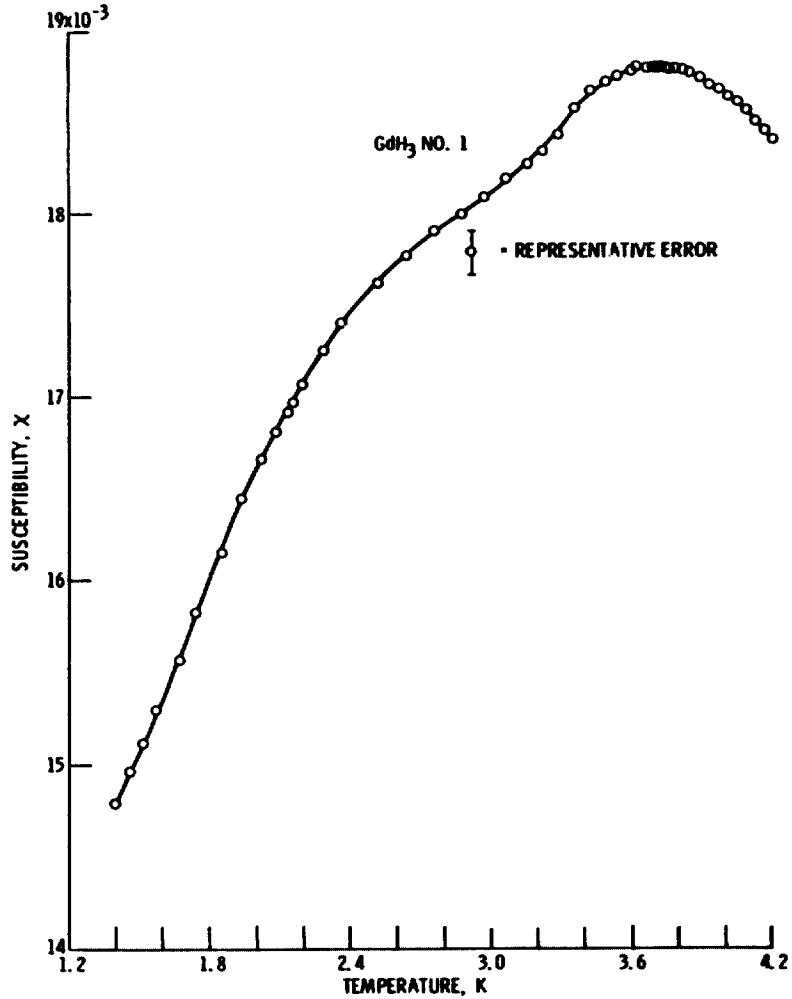

Figure 2. - Differential magnetic susceptibility of GdH_3 versus temperature.

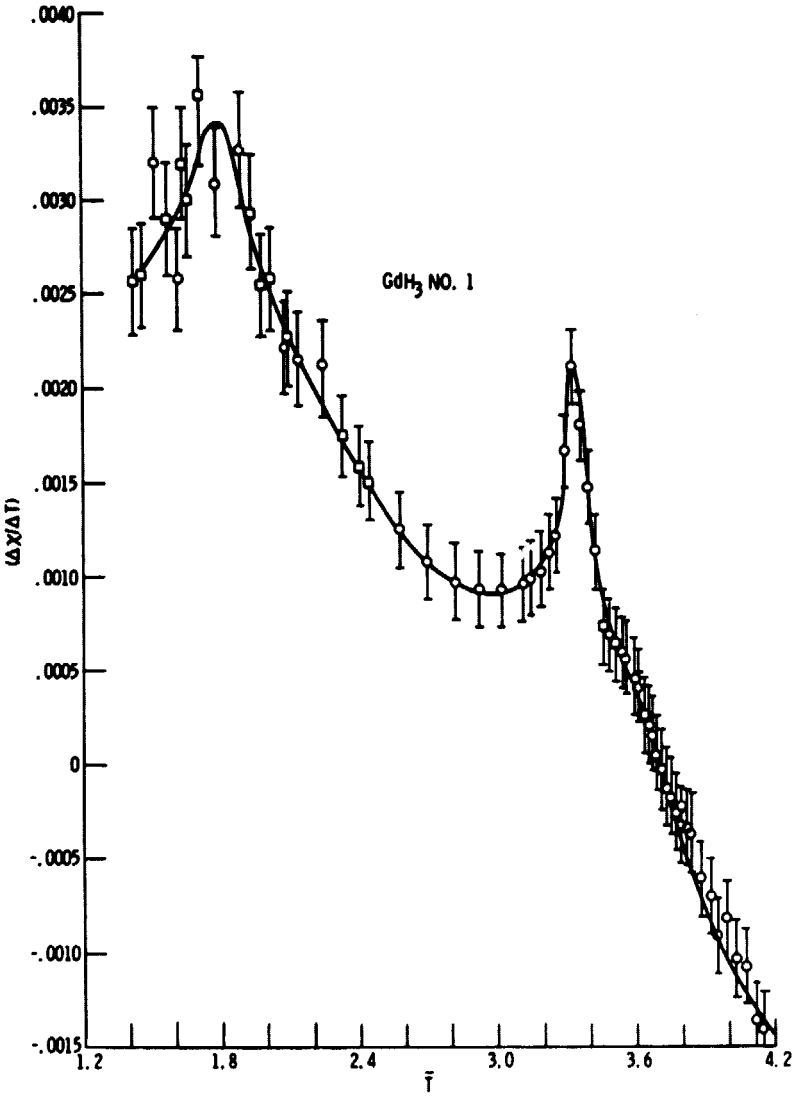

Figure 3. - $\Delta\chi/\Delta T$ versus temperature from figure 2 for GdH_3.

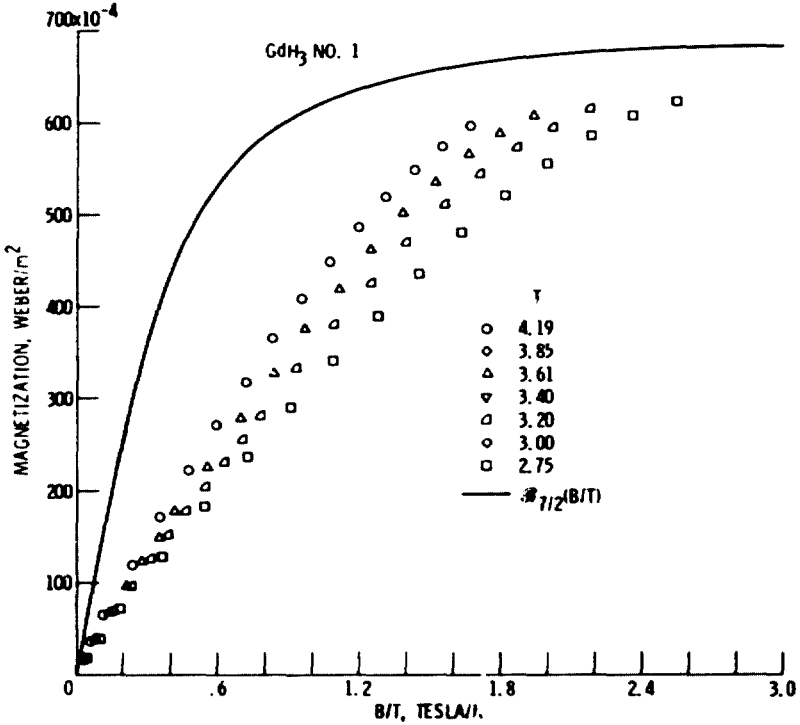

Figure 4. - Magnetization versus B/T for GdH_3. The solid curve is a plot of the magnetization given by $M = M_S \cdot \mathcal{B}_{7/2}(B/T)$ where $M_S = Ng_L\mu_B J$. N for the sample used was $(10.6 \pm 0.4) \times 10^{21}$ ions/cm^3.

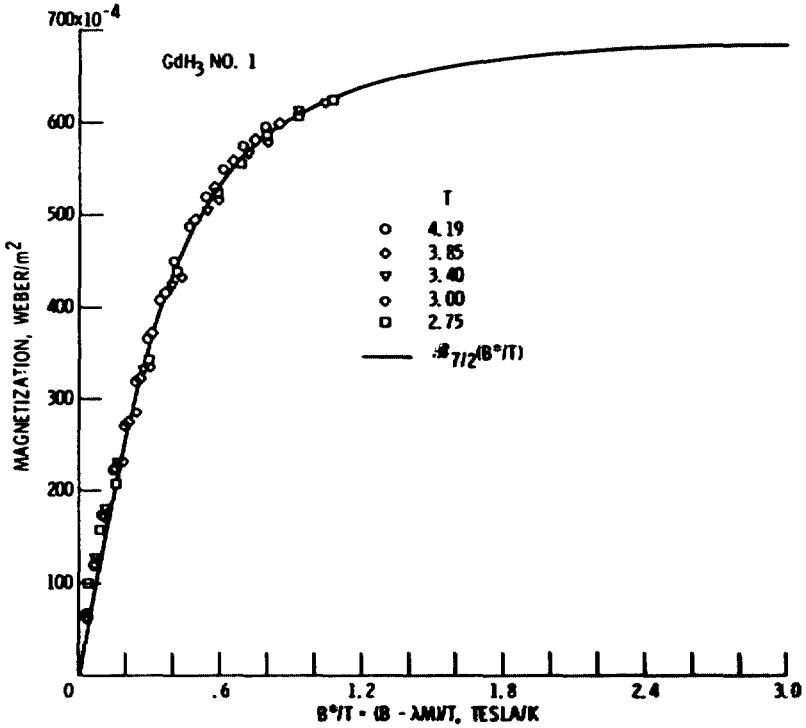

Figure 5. - Magnetization of GdH_3 as a function of $B^*/T = (B - \lambda M)/T$. λ is the Weiss molecular field constant.

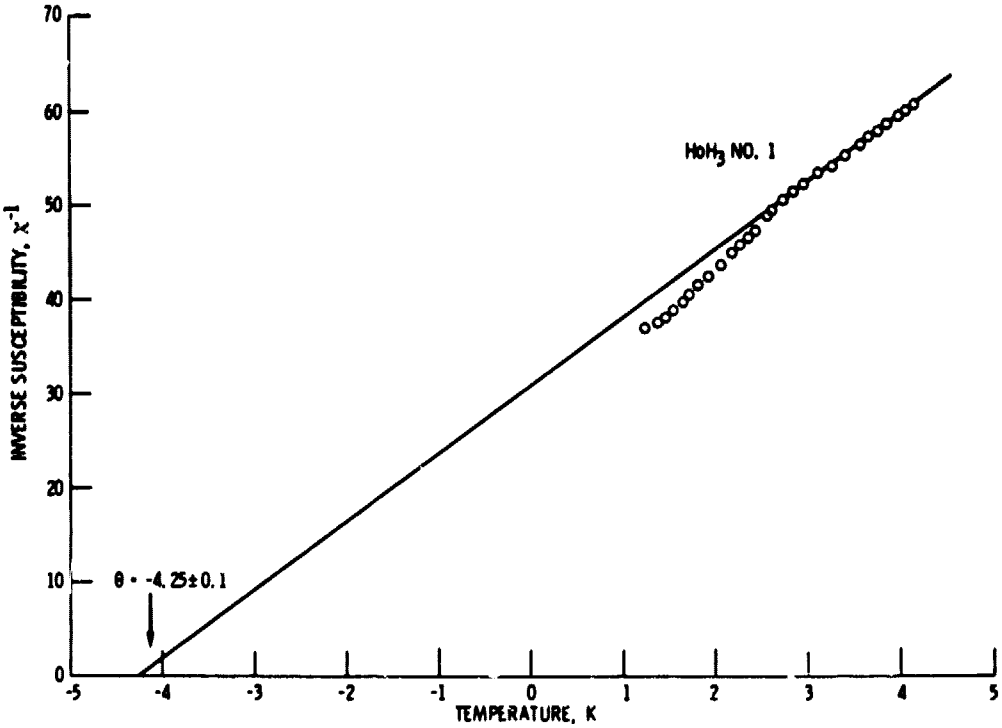

Figure 6. - Inverse differential magnetic susceptibility versus temperature for HoH_3. $N = (9.44 \pm 0.38) \times 10^{21}$ ions/cm^3.

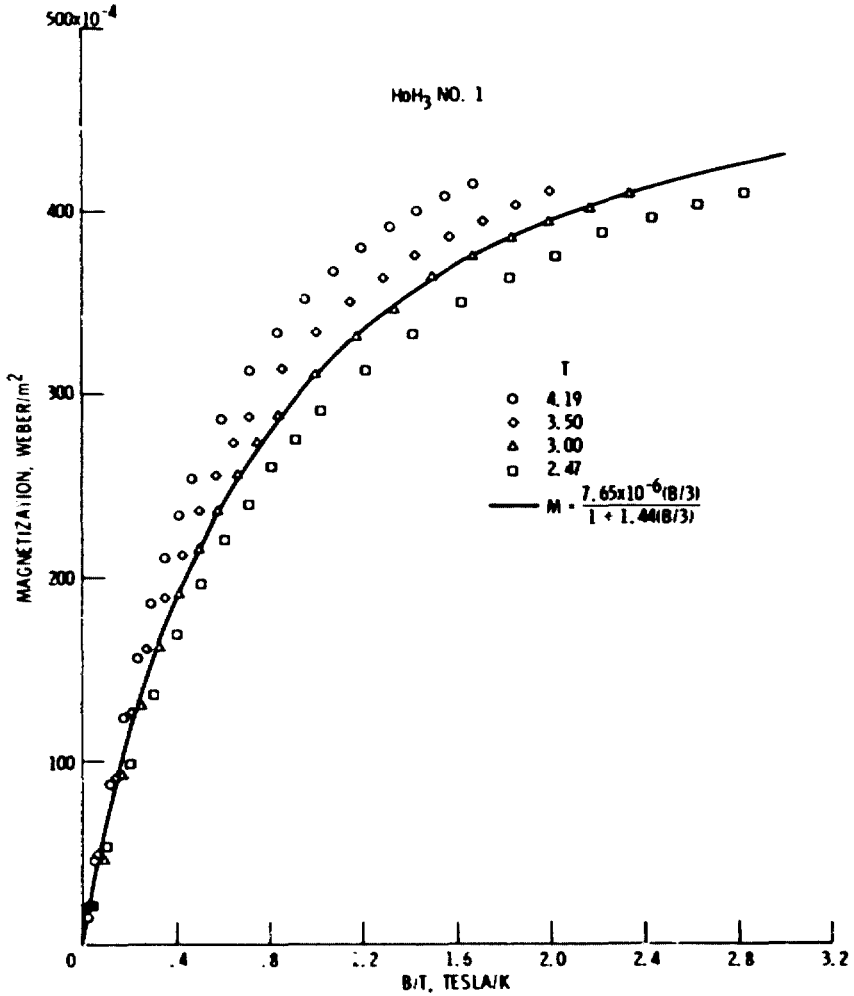

Figure 7. Magnetization of HoH_3 as a function of B/T. The solid curve is the expression $M = (7.65\times10^{-3}\ B/T)/(1 + 1.44\ B/T)$, chosen to fit the data at $T = 3$ K. Similar fits to the data at other temperatures predict, within experimental error, the same saturation magnetization.

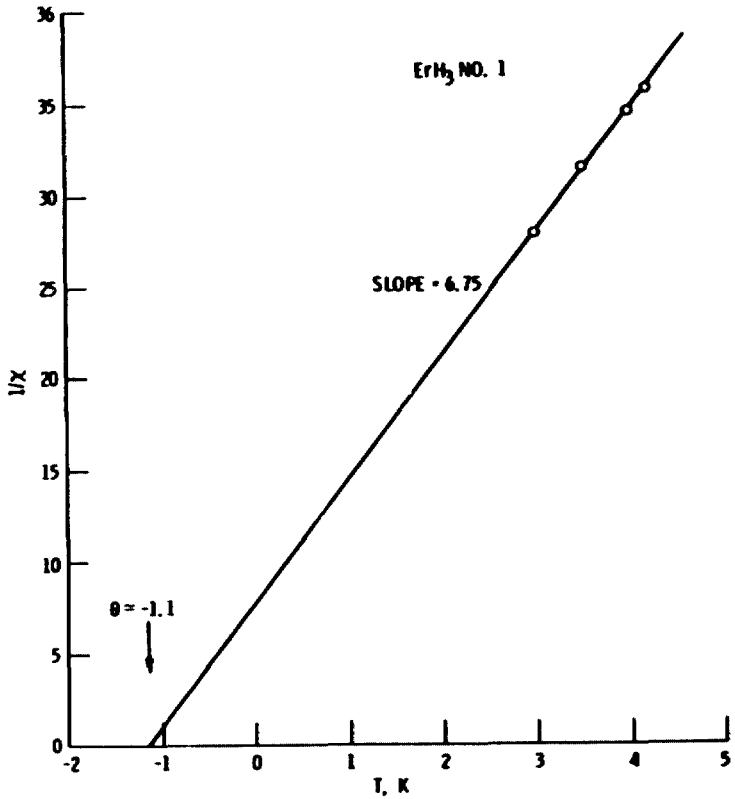

Figure 8. - Magnetic susceptibility from initial slopes of M versus B for ErH_3 as a function of temperature. $N = (12.11 \pm 0.48)\times10^{21}$ ions/cm^3.

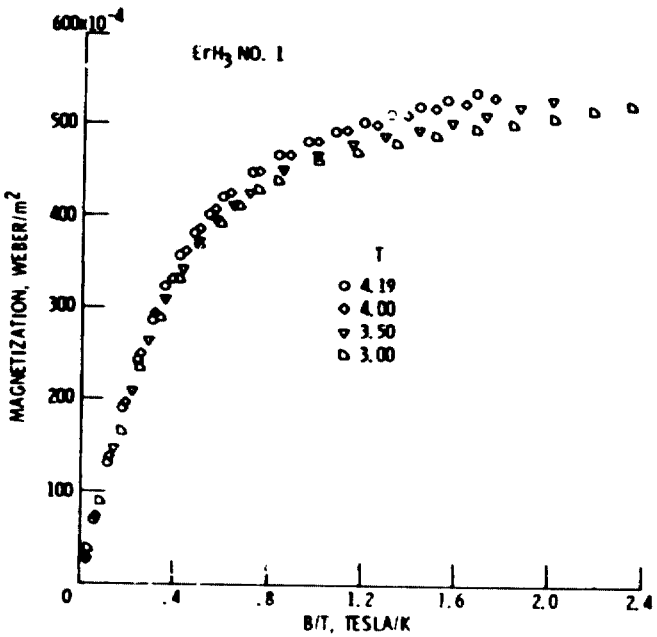

Figure 9. - Magnetization of ErH_3 as a function of B/T.

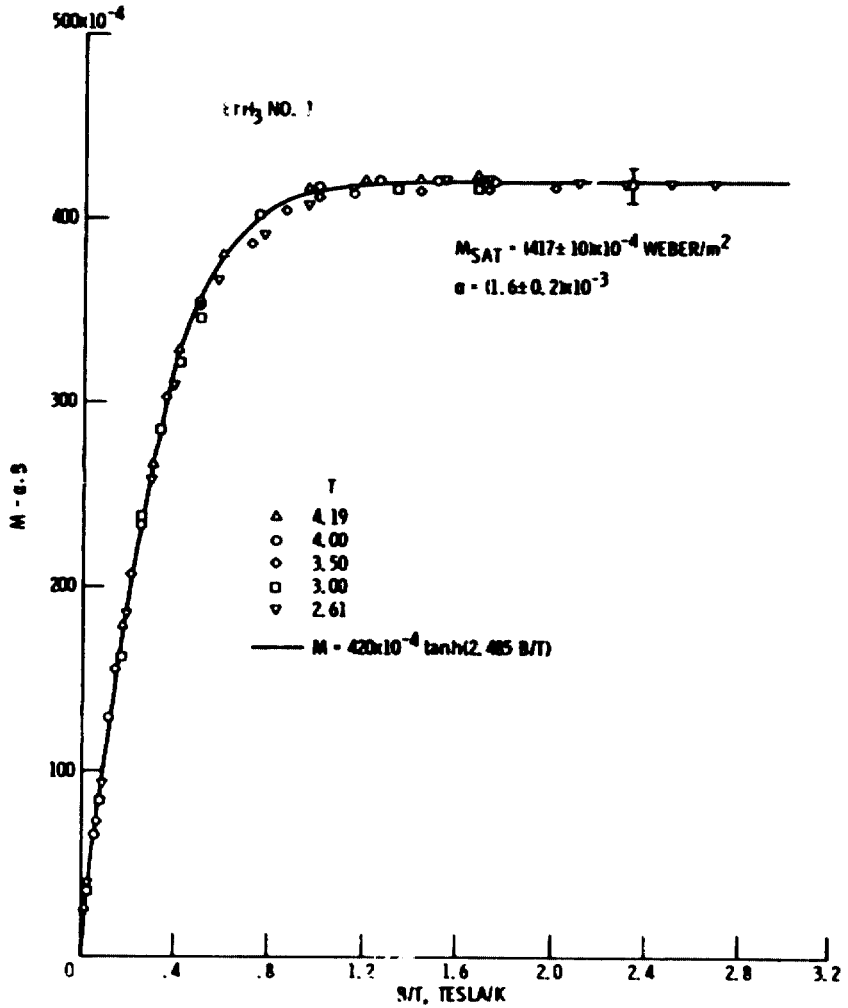

Figure 10. - Magnetization of ErH_3 with the temperature-independent contribution subtracted from the experimental data. The slope of the van Vleck contribution is 1.6×10^{-3} Weber/m^2/Tesla.

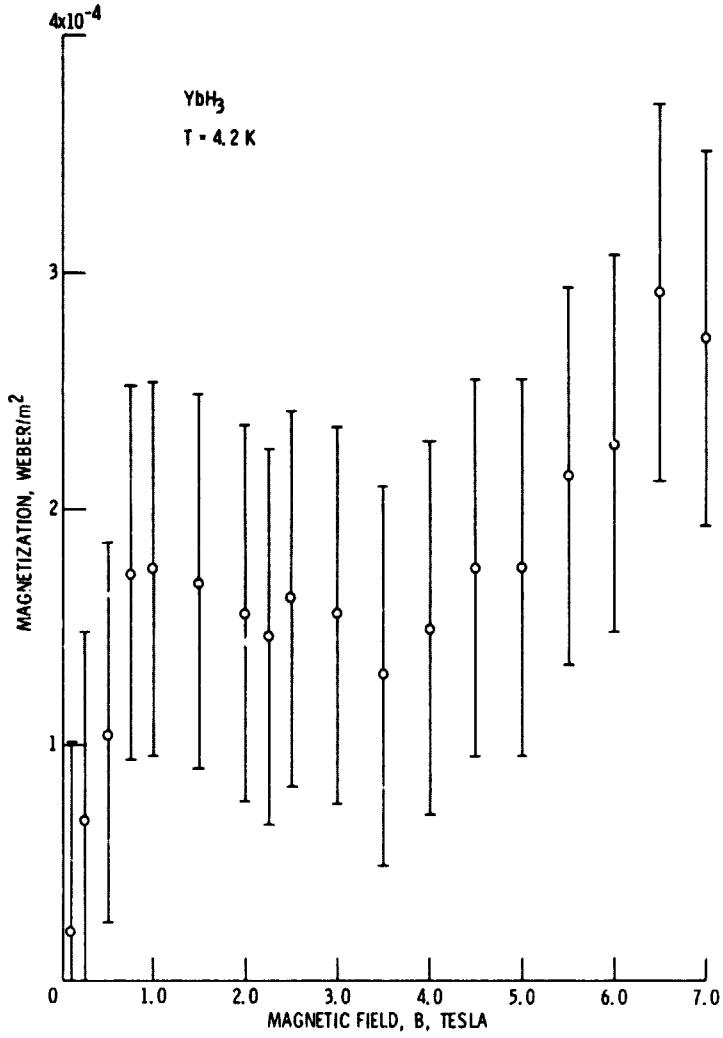

Figure 11. - Magnetization of YbH_3 as a function of applied field at T = 4.2 K.